

A Tempo-Spatial Compressed Sensing Architecture for Efficient High-throughput Information Acquisition in Organs-on-a-chip

Chen Song¹, Aosen Wang¹, Feng Lin¹, Ruogang Zhao², Zhanpeng Jin³, Wenyao Xu¹

Abstract—As a microengineered biomimetic system to replicate key functions of living organs, organs-on-a-chip (OC) technology provides a high-throughput model for investigating complex cell interactions with a high temporal and spatial resolution in biological studies. Typically, microscopy and high-speed video cameras are used for data acquisition, which are expensive and bulky. Recently, compressed sensing (CS) has increasingly attracted attentions due to its extremely low-complexity structure and low sampling rate. However, there is no CS solution tailored for tempo-spatial information acquisition. In this paper, we propose Tempo-Spatial CS (TS-CS), a unified CS architecture for OC stream which achieves significant cost reduction and truly combines sensing with compression along the temporal and spatial domains. We point out that TS-CS can consistently achieve better performance by exploiting tempo-spatial compressibility in OC data. To this end, we present TS-CS architecture and comprehensively evaluate the system performance. With comparison to the traditional way, we show that TS-CS always obtains better recovery result with a throughput bound and can achieve around 25% throughput improvement under a reconstruction demand.

I. INTRODUCTION

Organs-on-a-chip (OC) is a newly emerged technology that seeks to recapitulate the structure and physiological function of native human organs using miniaturized in vitro 3D culture of living cells, and has been envisioned as a promising platform for drug screening and disease modeling in point-of-care (POC) applications [1], [2]. Existing OC devices are mostly made of optical-transparent, biocompatible Polydimethylsiloxane (PDMS) material. In biomedical research, an in vitro model system with the potential to replace resource-limited animal and human experimentation is of high interest. This has been traditionally addressed by centimeter-sized three-dimensional engineered tissues. However, these large constructs typically require millions of cells, have a steep gradient of cell density from the surface to the core, and face diffusional limitations of oxygen and media exchange. Due to its miniature size, OC model overcomes the difficulties above, while also offering orders of magnitude scale-up advantages over conventional engineered tissues in terms of homogeneity of cell sources and the number of conditions that can be studied in parallel.

¹C. Song, A. Wang, F. Lin, and W. Xu are with the Department of Computer Science and Engineering, University at Buffalo (SUNY), Buffalo, NY 14260, USA {csong5, aosenwan, flin28, wenyaoxu}@buffalo.edu

²R. Zhao is with the Department of Biomedical Engineering, University at Buffalo (SUNY), Buffalo, NY 14260, USA rgzhao@buffalo.edu

³Z. Jin is with the Department of Electrical and Computer Engineering, Binghamton University (SUNY), Binghamton, NY 13902, USA zjin@binghamton.edu

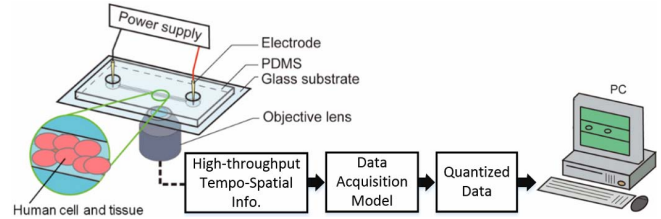


Fig. 1. Overview of human organs-on-a-chip.

Fig. 1 shows an overview of human organs-on-a-chip. The microfluidic culture device synthesizes minimal functional organ units that recapitulate tissue- and organ-level functions in PDMS. The entire movements are then recorded by Data Acquisition Model (DAM) through the lens. In order to achieve the high-resolution, real-time information, the current DAM deploys the high-resolution microscopy and the high-speed camera, which are expensive and bulky. A low-cost, low-complexity and high-performance DAM solution is urgently demanded to enable POC application of OC.

Compressed Sensing (CS) [3] has achieved significant development in recent years. It is an efficient Analog-to-Information (A2I) framework that simultaneously combines sampling and compression into a single process. Inspired by the work of Duarte *et al.* [4], where a simpler, smaller, and cheaper single pixel camera architecture was presented based on CS, we explore the possibility of applying CS on organ-on-a-chip data acquisition.

Traditional CS approaches usually focus on single data domain, either in spatial (still images [5]) or in temporal (bio channel signals [6]). Some CS strategies have been proposed for the high-throughput video stream. Reddy *et al.* [7] applied a random mask on each frame and reduced the temporal frames by integrating several encoded frames together before spatial downsampling. Since it only aggregates a certain number of frames along the temporal domain, P2C2 is essentially a spatial-based CS scheme. Sankaranarayanan *et al.* [8] located similar frames in the video via motion estimation to achieve temporal downsampling, which means the architecture still needs to measure each frame individually at specific resolution. To the best of our knowledge, there is no similar unified CS architecture for Tempo-Spatial stream that can truly complete the sensing and compression at the same time in the front-end.

In this paper, we present, TS-CS, a novel unified CS architecture for high-throughput OC information collection. TS-CS is a better DAM approach in terms of complexity and cost. It provides better compression-performance tradeoff by efficiently compressing and sensing the OC data in both

temporal and spatial domains. With TS-CS, the traditionally expensive and bulky OC DAM can be replaced by the low-cost and low-complexity devices.

II. TS-CS ARCHITECTURE

A. Compressed Sensing Background

Compressed sensing (CS) is a new emerging low-rate sampling scheme which deals with the estimation of a K -sparse signal $x \in \mathbb{R}^N$ from a non-adaptive measurement vector $y \in \mathbb{R}^M$, where $K < M \ll N$. Given a sensing matrix Φ with Restricted Isometry Property [3] and $M \sim K \log(\frac{N}{K})$, the signal x can be recovered with high possibility by solving the following ℓ_1 -norm minimization problem:

$$\arg \min_x \|x\|_1 \quad s.t. \quad \|y - \Phi x\|_2 \leq \epsilon, \quad (1)$$

where ϵ is the reconstruction error tolerance.

In practice, the signal x is most likely not sparse but with respect to some certain sparsity-inducing basis Ψ . Then the problem becomes:

$$\arg \min_{\hat{x}} \|\hat{x}\|_1 \quad s.t. \quad \|y - \Phi \Psi \hat{x}\|_2 \leq \epsilon. \quad (2)$$

After recovering \hat{x} , we estimate the original signal x :

$$x_{rec} = \Psi \hat{x}. \quad (3)$$

B. TS-CS Architecture Overview

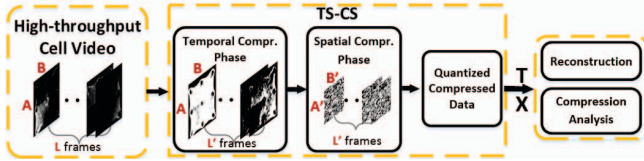


Fig. 2. The overview of TS-CS architecture.

While the existing CS approaches for high-throughput stream mostly focus in the single domain, we propose TS-CS, a unified CS architecture which combines temporal compression and spatial compression together before quantization. We term the video stream in the form of $f \times r \times c$, while f is the number of the frames and $r \times c$ is the size of each frame. Fig. 2 shows the overview of the whole dataflow. The original high-throughput OC stream S is in the size of $L \times A \times B$. TS-CS compresses the steam in two domains and outputs the compressed data in the size of $L' \times A' \times B'$. After digital quantization, the data is transmitted for reconstruction or compression analysis. As depicted in Fig. 2, TS-CS mainly consists of two phases: Temporal Compression Phase and Spatial Compression Phase, where the data in the corresponding domain is compressed.

1) *Temporal Compression Phase*: The goal of this phase is to compress S from L into \hat{L} frames along the temporal domain ($\hat{L} < L$). Since the neighboring frames contain the continuous information of the organ movement, we can assume that each pixel array $P_{ab} = \{p_{ab}^1, \dots, p_{ab}^L\}$ along the temporal domain can be sparsely represented under a certain basis ($1 \leq a \leq A, 1 \leq b \leq B$).

Following the above assumption, we employ a $\hat{L} \times L$ sensing matrix, M , to reduce the dimension of each P_{ab}

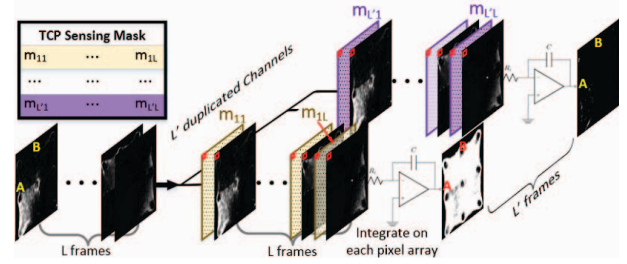


Fig. 3. The structure of Temporal Compression Phase.

in the temporal domain. To achieve that, we duplicate S into \hat{L} channels (see Fig. 3), while $\{TCP^i | 1 \leq i \leq \hat{L}\}$ denotes the output frame of the i th channel. In each channel i , the corresponding i th row in M is applied to modulate each P_{ab} . Let m_{ij} be the entry at the i th row and j th column in M . By integrating L modulated frames, we calculate each pixel in the output matrix as:

$$TCP_{ab}^i = \sum_{j=1}^L p_{ab}^j \times m_{ij}, \forall 1 \leq i \leq \hat{L}, 1 \leq a \leq A, 1 \leq b \leq B. \quad (4)$$

In this way, we apply CS along the temporal domain and obtain \hat{L} frames instead of the original L ones after Temporal Compression Phase. Note that although each TCP^i still remains the size of $A \times B$, the information contained is actually the fusion of the original L frames.

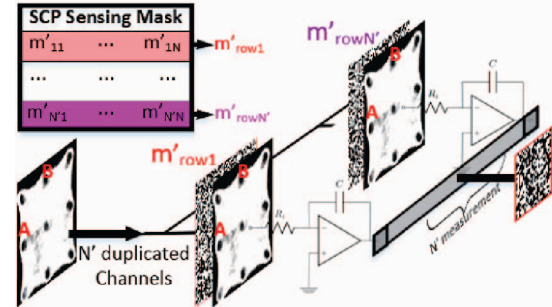


Fig. 4. The structure of Spatial Compression Phase.

2) *Spatial Compression Phase*: In this phase, we conduct compression in the spatial domain to compress the size of each TCP^i from $N = A \times B$ to $N' = A' \times B'$. Specifically, we generate an $N' \times N$ sensing matrix, M' , for the spatial dimension reduction. For each TCP^i (see Fig. 4), we duplicate the frame into N' channels. In each channel i , we set the corresponding i th row in M' to modulate the whole frame. For the ease of representation, let $TCP^{t,i}$ be the vectorized form ($N \times 1$ array) of TCP^i , m'_{ij} be the entry at the i th row and j th column in M' and SCP^i be the modulation result of TCP^i after Spatial Compression Phase. The final measurement in each channel i is the integration of all the modulated pixel values, which is formulated as:

$$SCP_t^i = \sum_{j=1}^N TCP_j^{t,i} \times m'_{ij}, \forall 1 \leq t \leq N', 1 \leq i \leq \hat{L}. \quad (5)$$

Eventually, after converting the result SCP^i from $N' \times 1$ to $A' \times B'$, we successfully compress the data from $L \times A \times B$

data into $L' \times A' \times B'$ and the compression ratio (CR) is defined as $(L' \times A' \times B') / (L \times A \times B) \times 100\%$.

It is worth to mention that the duplicate-channel scheme is for the purpose of demonstration. In practice, a control unit can be applied to adjust the modulation mask via Digital Micromirror Device array (DMD) according to the sensing matrix at a rate higher than the acquisition frame rate of the camera. Both low frame-rate video camera and high frame-rate modulator (DMD) are inexpensive, which therefore results in a significant cost reduction.

3) *Reconstruction*: After receiving the compressed data at the receiver end, we apply the reconstruction algorithm to obtain the original OC stream in the size of $L \times A \times B$. Typically, the reconstruction procedure is in the reverse order of the compression, which means the reconstruction is conducted first in the spatial domain and then in the temporal domain by solving the ℓ_1 -norm minimization problem.

III. EXPERIMENTAL RESULTS

To evaluate the advantage of TS-CS, we use a real OC stream of size $34 \times 64 \times 64$. Microtissues are stained with immunofluorescence dyes for nuclei and collagen. The microtissues are then imaged on a Zeiss LSM-510 Meta confocal microscope with a Plan-Apochromat 20X air objective in $1.5\mu\text{m}$ optical slices for all channels. For each microtissue imaged, a $450\mu\text{m} \times 209\mu\text{m}$ area is scanned through an approximately $80\mu\text{m}$ thickness. The stack of images obtained in confocal microscopy is used as original OC data.

We implement TS-CS architecture as well as the traditional CS approach (denoted as Tra-CS), which individually applied CS on each frame. We generate the random Bernoulli matrix to be the sensing matrix Φ and employ inverse discrete cosine transform matrix as the basis Ψ . Let TCS and SCS be the measurement settings in Temporal Compression Phase and Spatial Compression Phase. In TS-CS, the combination of 10 TCS ([1, 4, 7, 10, 13, 16, 19, 22, 25, 28]) and 30 SCS (from 100 ~ 3000 with the step of 100) are simulated. The same 30 SCS are simulated with Tra-CS. The recovery error is measured by Signal to Noise and Distortion Ratio (SNDR):

$$SNDR = 20 \log \frac{\|x_t\|_2}{\|x_t - \hat{x}_t\|_2}, \quad (6)$$

where x_t is the original vectorized frame and \hat{x}_t is the reconstructed one. Specifically, we calculate the average SNDR of 34 frames.

A. Reconstruction Result of TS-CS with TCS and SCS

We explore the reconstruction result of TS-CS when applying different TCS and SCS. We group the results in terms of TCS and only show partial results here for the purpose of visualization. As shown in Fig. 5, the average SNDR gradually grows when CR increases (choose larger SCS) under a given TCS. The performance experiences fluctuation when TCS is relatively small (e.g., TCS=4). This is understandable because smaller TCS means fewer measurements of each pixel array in the temporal domain. However, when TCS keeps increasing, the performance improves in a steady

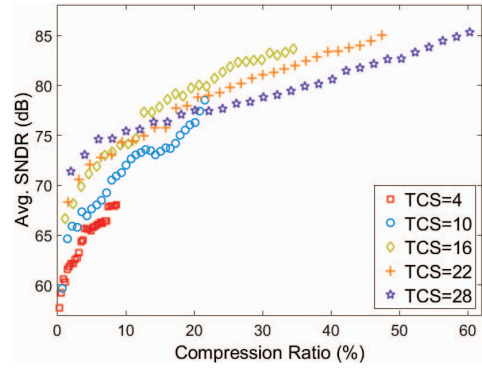


Fig. 5. The reconstruction result of TS-CS with different TCS and SCS.

way despite some minor variations, which can be introduced by the random sensing matrix and reconstruction algorithm.

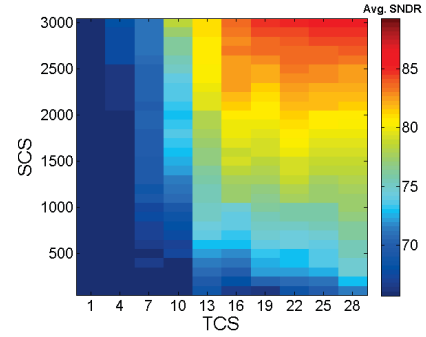


Fig. 6. The heatmap of the reconstruction result of TS-CS.

Fig. 6 depicts the heatmap of the reconstruction result under different TCS/SCS. The color in each grid is correlated to SNDR under the corresponding setting. Generally, the reconstruction performance improves with the increase of TCS and SCS. The top right corner with larger TCS and SCS achieves better performance compared with the rest.

B. Comparison between TS-CS and Tra-CS

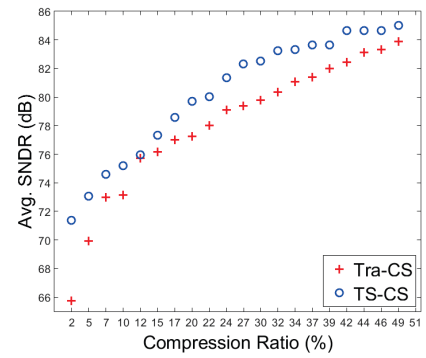


Fig. 7. Reconstruction comparison between TS-CS and Tra-CS.

To compare TS-CS with the traditional one in terms of reconstruction result, we first simulate Tra-CS on each frame with 20 different SCS, resulting in 20 reference CR and SNDR. We set each CR as the upper bound, and search for all the possible TCS/SCS pairs in TS-CS that have a smaller CR. Within all the pairs found, we choose the pair with the best performance as the optimal pair and compare it to the performance of Tra-CS. As shown in Fig. 7, the

reconstruction result of Tra-CS is plotted in red cross and the corresponding TS-CS optimal pair is plotted in blue circle. We can see that TS-CS achieves better recovery result than Tra-CS along all SCS (100 ~ 2000). Specifically, we define the performance improvement as:

$$REC_{enhance} = \frac{SNDR(TS-CS) - SNDR(Tra-CS)}{SNDR(Tra-CS)}. \quad (7)$$

As a result, TS-CS outperforms Tra-CS up to 8.6% in terms of SNDR. With the above observation, we can prudentially draw a conclusion that given a CR upper bound, there is always a pair of TCS/SCS in TS-CS that can achieve better performance than Tra-CS.

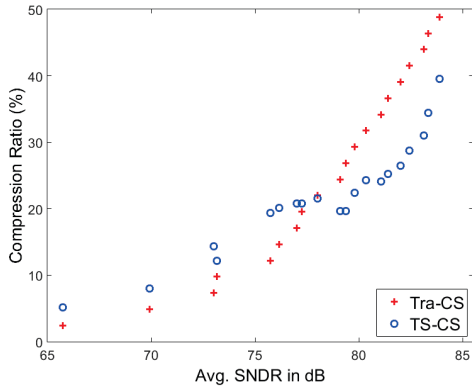


Fig. 8. The comparison between TS-CS and Tra-CS in terms of throughput.

We also compare the throughput between TS-CS and Tra-CS. With 20 SNDR in Tra-CS obtained above, we set each as the performance lower bound, and search for all the possible TCS/SCS pairs in TS-CS that obtain higher average SNDR. Within all the pairs found, we select the pair with the smallest CR as the optimal pair in the study.

As shown in Fig. 8, the results can be categorized into two cases. When the performance bound is small (average SNDR < 78), the closest performance is achieved with small CR ($\leq 20\%$), which can lead to larger performance fluctuation and additional recover error because there are two reconstruction steps in TS-CS. These variations cause the result that the CR of the optimal pair in TS-CS is larger than the reference one in Tra-CS. However, when the performance bound is larger than a certain threshold (average SNDR > 78), the optimal pair in TS-CS consistently obtains a smaller CR than Tra-CS (smaller CR means larger throughput). Particularly, we define the throughput enhancement as:

$$TP_{enhance} = \frac{CR(Tra-CS) - CR(TS-CS)}{CR(Tra-CS)} \times 100\%. \quad (8)$$

TS-CS achieves an average throughput improvement of 25% over Tra-CS. The higher throughput means more data acquisition and less energy consumption in transmission.

C. Case Study

In Fig. 9, we demonstrate the real OC stream as well as the reconstructed ones from TS-CS. Only partial frames are selected due to space limit. As can be seen, the original data records the entire organ movement. With $CR \approx 60.3\%$,

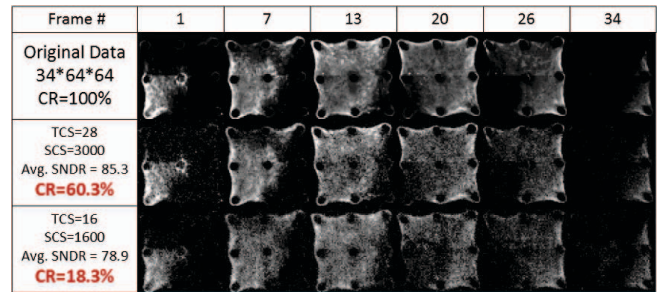


Fig. 9. A demonstration of the real OC data and the reconstructed ones by TS-CS.

the reconstructed frames of TS-CS can precisely reserve the details of the original ones. If we keep reducing CR down to $\approx 18.3\%$, TS-CS can still achieve reliable performance, as the whole movement pattern can be clearly observed. Therefore, TS-CS is a promising high-throughput architecture for OC data acquisition.

IV. CONCLUSION

We presented TS-CS, a novel A2I architecture for high-throughput organ-on-a-chip video which combines sensing with compression along the temporal and spatial domains, and validated its performance using the real OC data. TS-CS can be seamlessly integrated with other advanced CS technologies with regard to different practical scenarios, such as signal dynamics [9], [10], quantization effect [11] and architecture configuration [12], [13].

REFERENCES

- [1] S. N. Bhatia *et al.*, “Microfluidic organs-on-chips,” *Nature biotechnology*, 2014.
- [2] D. Huh *et al.*, “Microengineered physiological biomimicry: organs-on-chips,” *Lab on a chip*, vol. 12, no. 12, pp. 2156–2164, 2012.
- [3] D. L. Donoho, “Compressed sensing,” *Information Theory, IEEE Transactions on*, vol. 52, no. 4, pp. 1289–1306, 2006.
- [4] M. F. Duarte *et al.*, “Single-pixel imaging via compressive sampling,” *IEEE Signal Processing Magazine*, vol. 25, no. 2, p. 83, 2008.
- [5] M. Lustig *et al.*, “Sparse mri: The application of compressed sensing for rapid mr imaging,” *Magnetic resonance in medicine*, vol. 58, no. 6, pp. 1182–1195, 2007.
- [6] T. Xiong *et al.*, “A dictionary learning algorithm for multi-channel neural recordings,” in *IEEE Biomedical Circuits and Systems Conference (BioCAS)*, 2014, pp. 9–12.
- [7] D. Reddy *et al.*, “P2C2: Programmable pixel compressive camera for high speed imaging,” in *IEEE Conference on Computer Vision and Pattern Recognition (CVPR)*, 2011, pp. 329–336.
- [8] A. C. Sankaranarayanan *et al.*, “CS-MUVI: Video compressive sensing for spatial-multiplexing cameras,” in *IEEE International Conference on Computational Photography (ICCP)*, 2012, pp. 1–10.
- [9] A. Wang *et al.*, “Adaptive compressed sensing architecture in wireless brain-computer interface,” in *ACM/IEEE Annual Design Automation Conference*, 2015, p. 173.
- [10] A. Wang *et al.*, “Ultra-low power dynamic knob in adaptive compressed sensing towards biosignal dynamics,” *IEEE Trans. on Biomed. Cir. and Sys.*, vol. 10, no. 3, pp. 579–592, June 2016.
- [11] A. Wang *et al.*, “Quantization effects in an analog-to-information front end in eeg telemonitoring,” *IEEE Trans. on Cir. and Sys. II*, vol. 62, no. 2, pp. 104–108, 2015.
- [12] A. Wang *et al.*, “A configurable quantized compressed sensing architecture for low-power tele-monitoring,” in *IEEE International Green Computing Conference (IGCC)*, 2014, pp. 1–10.
- [13] A. Wang *et al.*, “A configurable energy-efficient compressed sensing architecture with its application on body sensor networks,” *IEEE Trans. on Industrial Informatics*, vol. 12, no. 1, pp. 15–27, 2016.